PROCEEDINGS OF SCIENCE

The Belle II Silicon Vertex Detector: Performance and Running Experience

S. Bacher[w,*], K. Adamczyk[w], H. Aihara[s], T. Aziz[k], S. Bahinipati[g], G. Batignani[l,m], J. Baudot[f], P. K. Behera[h], S. Bettarini[l,m], T. Bilka[e], A. Bozek[w], F. Buchsteiner[b], G. Casarosa[l,m], D. Červenkov[e], Y. Q. Chen[d], L. Corona[l,m], T. Czank[r], S. B. Das[i], N. Dash[h], G. de Marino[A,l,m], Z. Doležal[e], G. Dujany[f], F. Forti[l,m], M. Friedl[b], E. Ganiev[n,o], B. Gobbo[o], S. Halder[k], K. Hara[t,p], S. Hazra[k], T. Higuchi[r], C. Irmler[b], A. Ishikawa[t,p], H. B. Jeon[u], Y. Jin[n,o], C. Joo[r], M. Kaleta[w], A. B. Kaliyar[k], J. Kandra[e], K. H. Kang[u], P. Kapusta[w], P. Kodyš[e], T. Kohriki[t], M. Kumar[i], R. Kumar[j], P. Kvasnička[e], C. La Licata[r], K. Lalwani[i], S. C. Lee[u], Y. B. Li[c], J. Libby[h], S. Maity[g], S. N. Mayekar[k], G. B. Mohanty[k], J. A. Mora Grimaldo[s], T. Morii[r], K. R. Nakamura[t,p], Z. Natkaniec[w], Y. Onuki[s], W. Ostrowicz[w], A. Paladino[l,m], E. Paoloni[l,m], H. Park[u], K. K. Rao[k], I. Ripp-Baudot[f], G. Rizzo[l,m], N. Rout[h], D. Sahoo[k], C. Schwanda[b], J. Suzuki[t], S. Tanaka[t,p], H. Tanigawa[s], R. Thalmeier[b], T. Tsuboyama[t,p], Y. Uematsu[s], O. Verbycka[w], L. Vitale[n,o], K. Wan[s], J. Webb[a], J. Wiechczynski[m], H. Yin[b], L. Zani[B,l,m] and T. Zhang[s]

(Belle-II SVD Collaboration)

[a] *School of Physics, University of Melbourne, Melbourne, Victoria 3010, Australia*
[b] *Institute of High Energy Physics, Austrian Academy of Sciences, 1050 Vienna, Austria*
[c] *Peking University, Department of Technical Physics, Beijing 100871, China*
[d] *University of Science and Technology of China, Department of Modern Physics, Hefei 230026, China*
[e] *Faculty of Mathematics and Physics, Charles University, 121 16 Prague, Czech Republic*
[f] *IPHC, UMR 7178, Université de Strasbourg, CNRS, 67037 Strasbourg, France*
[g] *Indian Institute of Technology Bhubaneswar, Satya Nagar, India*
[h] *Indian Institute of Technology Madras, Chennai 600036, India*
[i] *Malaviya National Institute of Technology Jaipur, Jaipur 302017, India*
[j] *Punjab Agricultural University, Ludhiana 141004, India*
[k] *Tata Institute of Fundamental Research, Mumbai 400005, India*
[l] *Dipartimento di Fisica, Università di Pisa, I-56127 Pisa, Italy,* [A] *presently at Université Paris-Saclay, CNRS/IN2P3, IJCLab, 91405 Orsay, France,* [B] *presently at Aix Marseille Univ, CNRS/IN2P3, CPPM, 13288 Marseille, France*
[m] *INFN Sezione di Pisa, I-56127 Pisa, Italy*
[n] *Dipartimento di Fisica, Università di Trieste, I-34127 Trieste, Italy*
[o] *INFN Sezione di Trieste, I-34127 Trieste, Italy*

[*] Speaker

PoS(ICHEP2020)718

[p] *The Graduate University for Advanced Studies (SOKENDAI), Hayama 240-0193, Japan*
[r] *Kavli Institute for the Physics and Mathematics of the Universe (WPI), University of Tokyo, Kashiwa 277-8583, Japan*
[s] *Department of Physics, University of Tokyo, Tokyo 113-0033, Japan*
[t] *High Energy Accelerator Research Organization (KEK), Tsukuba 305-0801, Japan*
[u] *Department of Physics, Kyungpook National University, Daegu 41566, Korea*
[w] *H. Niewodniczanski Institute of Nuclear Physics, Krakow 31-342, Poland*

E-mail: sbacher@ifj.edu.pl

In spring 2019 the fully equipped Belle II experiment started data taking at the energy of the Y(4S) resonance. The new vertex detector (VXD) consists of two inner layers of DEPFET pixels (PXD) and four outer layers of double-sided silicon strip detectors (SVD). It plays a crucial role in recording high-quality data in the new high-luminosity environment of the SuperKEKB collider, characterized by severe beam backgrounds. The SVD was operated reliably during the 2019 physics run, showing high stability of the noise levels and calibration parameters. The SVD performance, measured with first data, showed excellent hit and tracking efficiencies, high signal-to-noise ratio, and cluster energy distribution in fair agreement with the expectations. Detailed studies of the good spatial resolution achieved will be shown. The excellent hit-time resolution has also been measured, which will be exploited for background rejection in the coming years of running at higher luminosity.

40th International Conference on High Energy physics - ICHEP2020
July 28 - August 6, 2020
Prague, Czech Republic (virtual meeting)

1. Introduction

In quest of a new physics beyond the Standard Model, the Belle II experiment [1] started data taking at the SuperKEKB collider [2] in Tsukuba, Japan in March 2019. The e^+e^- collider is tuned for production of B meson pairs, with center-of-mass energy of Y(4S) resonance (10.58 GeV). We plan to collect 50 ab^{-1} data in ten years of operation from now.

The innermost part of the Belle II detector is a cylindrically shaped 6-layer Vertex Detector (VXD). The first two layers are built of the DEPFET-based silicon pixel detector (PXD), and next four layers contain double-sided silicon strip detectors (DSSD), the Silicon Vertex Detector (SVD).

2. SVD Overview

The SVD layers are at radii of 39 mm, 80 mm, 104 mm, 135 mm, numbered from 3 to 6, as shown at a schematic drawing in Fig.1. The individual layers are composed of 7, 10, 12 and 16 ladder-like arrays of 2 to 5 DSSDs. In layers 4-6 forward sensors are slanted inwards to minimize the material crossed by particles moving in the direction of e^-. A photo of a half of SVD combined with PXD is shown in Fig.2.

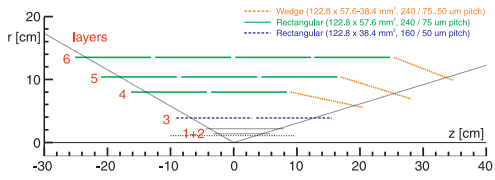

	Small	Large	Trapezoidal
# of p-strips*	768	768	768
p-strip pitch*	50 µm	75 µm	50-75 µm
# of n-strips*	768	512	512
n-strip pitch*	160 µm	240 µm	240 µm
thickness	320 µm	320 µm	300 µm
manufacturer	HPK		Micron

Figure 1: Dimensional details of SVD layout and its DSSDs.

As shown in Fig.1, three different shapes of DSSD are used: small and large rectangular sensors, and trapezoidal sensors. The small sensors are used in the layer 3, while a combination of the large and trapezoidal ones is used in other layers. The trapezoidal sensors are used in the forward, slanted part, and the rectangular sensors are used in the barrel part.

We define a global cylindrical coordinate system (r, ϕ, z), where the $+z$ direction is along the e^- beam direction, r is the radius, and ϕ is the azimuthal angle. Further, we define an extra, local coordinate system (u, v) on each sensor. The u (v) direction corresponds to the $r\phi$ (z) direction in global coordinate system, and is measured by p (n) strips.

Due to the harsh radiation environment around VXD, APV25 [3] chips where chosen as a readout ASIC. They are expected to tolerate 100 Mrad (tested up to 20 Mrad), and offer a shaping time of 50ns. A lot of attention was paid to minimize distance between the APV25 chips, and sensors. For all sensors on the layer 3, as well as for forward-most and backward-most sensors, the chips are placed at the edges of the ladder. For the barrel part of the layers 4-6 sensors are arranged according to the so-called "origami" chip-on-sensor concept, where the detector hit signals collected on the sensor back-side are transmitted to the APV25 ASICs through a flexible circuit bent from the back to the head side[4]. This approach is used to minimize capacitive noise.

Placing readout chips inside active volume presents cooling challenges that are tackled using two phase (gas-liquid) CO_2 cooling lines, with the temperature of -20 °C, running along all the chips, as shown in Fig.2.

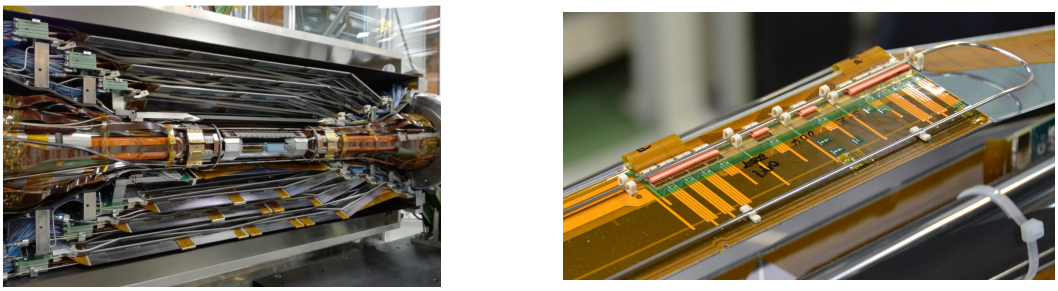

Figure 2: Left: Half of SVD detector, combined with PXD. Right: Cooling line on APV25 chips.

3. Stability and radiation effects

The SVD has operated smoothly since March 2019, when the data taking started. About 74.1fb^{-1} of e^+e^- collision data have been integrated so far, with peak instantaneous luminosity of (world record breaking) 2.4×10^{34}cm^{-2}s^{-1}.

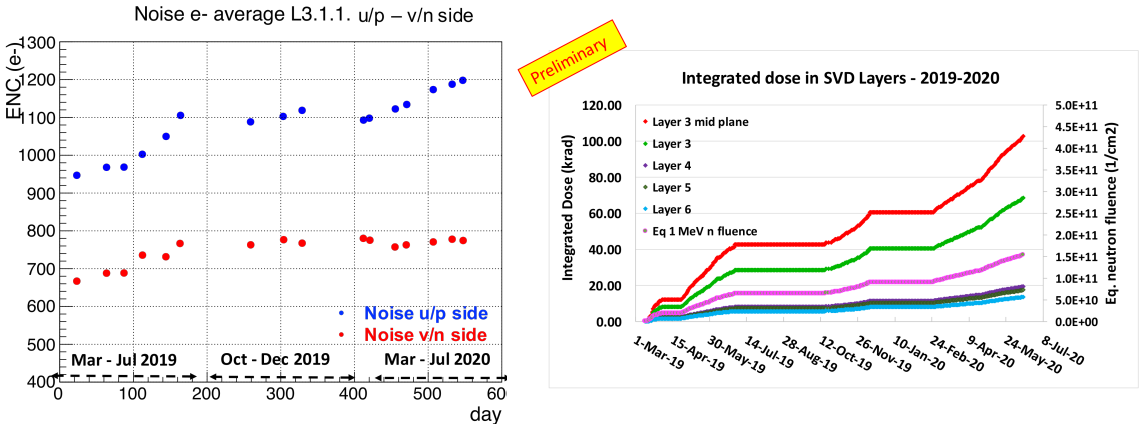

Figure 3: Noise (left) and integrated dose (right) trends since operation started in spring 2019.

In order to monitor the dose rate in the SVD, 20 diamond radiation sensors are located on the beam pipe and inside the SVD structure [5]. Using background simulation and correlating data taken by SVD and diamonds, it is possible to estimate the SVD dose rate and occupancy from diamond monitoring signals. This is used to track the SVD integrated dose also when the detector is not running, making it possible to generate plots as show in Fig.3.

As expected, both noise and leakage current increased along with the increase of integrated dose. The evolution of the noise with time, is shown in Fig.3. Some saturation of the noise increase is already visible on n-side and it is expected to happen also on p-side, since this effect is due to the initial increase of the fixed oxide charge on the sensor surface, induced by irradiation, that is also saturating with dose. For the layer 3, which is irradiated most severly, we observed leakage current increase from about $0.3\mu A$ to about $6\mu A$, in the 2019 run.

Despite the effects mentioned above, the performance of the SVD is not affected. For example, efficiency remains stable and well above 99%, as shown in Fig.4. We observed only $O(10)$ new

pinholes (localized defects in the oxide layer causing a short between the implant and the metal layer affecting single strips) during severe radiation accidents (quenches of superconducting quadrupole magnets of final focusing system). In total there are $O(1\%)$ masked channels in the SVD, and this number is stable since the beginning of the experiment, as those are mainly production defects.

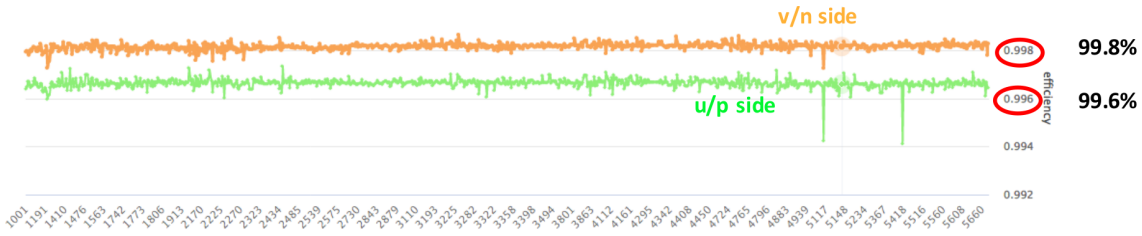

Figure 4: Average SVD efficiency plotted against run number in period between 2020-03-08 and 2020-06-15.

4. Performance

4.1 Cluster energy

In Fig.5 the distribution of the cluster energy of clusters used in tracking is shown for a few sensors in different positions. The energy of the cluster (E) depends on the track incident angle (α) through the (simplified) relation $E \simeq \frac{d}{sin\alpha} \cdot 80 \frac{e^-}{\mu m}$, where d is the sensor thickness in μm . Since the reconstructed tracks originates from the interaction point, their incident angles are different on sensors in different positions (see Fig.1 left), releasing more energy in the forward and backward sensors with respect to the sensors in the central part of the detector. The difference of the cluster energy on p and n sides of the same sensor is expected, and it's due to some charge loss on n side related to the presence of the floating strip combined with larger strip pitch of the n side..

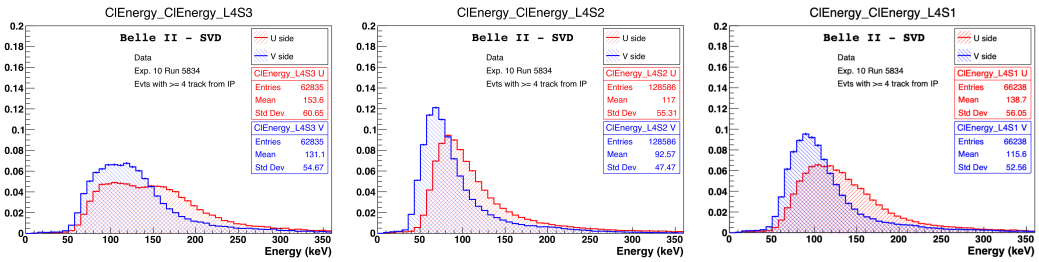

Figure 5: Energy cluster distribution on Layer 4.

4.2 Hit efficiency

Using reconstructed tracks, and calculating how often a cluster is found within ±0.5mm of said tracks, the efficiency is measured for every sensor. As shown in Fig.3, the average efficiency is stable above 99%. Only a few sensors with higher level of production defects exhibit lower values of about 98%.

4.3 Signal-to-noise ratio

The cluster signal-to-noise ratio is defined as $SNR = \frac{\Sigma_i S_i}{\sqrt{\Sigma_i N_i^2}}$, where $S_i(N_i)$ is the signal (noise) on the ith strip included in the cluster. The resulting SNR is very well within our expectations, ranging from 13 to 33. A few examples of SNR distribution are shown in Fig.6.

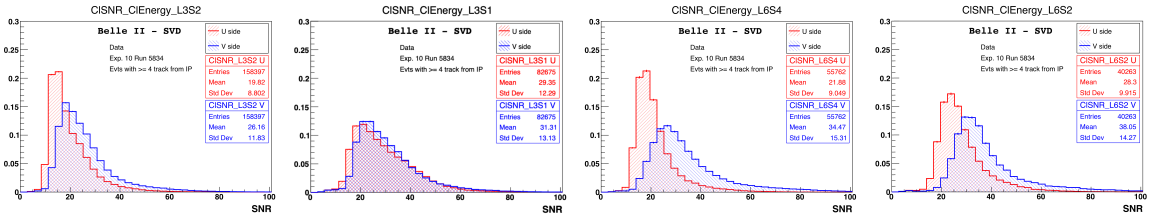

Figure 6: SNR distribution for a few sensors. The difference between the u and v side is due to the presence of the floating strip, and the different pitch of the two sides.

4.4 Spatial resolution

The spatial resolution is extracted in di-muon events, measuring the distance between the cluster position and the expected position of the track intercept. The cluster under investigation is excluded in the fitting of the tracks. In Fig.7 (left) we report the extracted position resolution as a function of the track incident angle for the two sides of the innermost layer. The resolution achieved on the v side is in fair agreement with expectations, while on the u side, with a resolution below $20\mu m$, there is room for an improvement of the software algorithms.

4.5 Hit-time resolution

The strip time is obtained as the calibrated centre-of-gravity of the 3 samples near the waveform peak [3] among the 6 provided by the APV255 (sampled every 31 ns), while the cluster time is the weighted average of the strip time with the strip charge. The cluster time distribution in candidate hadronic events for all clusters and clusters used in tracking is reported in Fig.7 (right), where the cluster time is referenced to the event time provided by the drift chamber. The achieved resolution is better than 3 ns, providing a powerful tool to reduce the background clusters, i.e. clusters produced by machine background off-time with respect to the triggered event. This is going to be particularly important for the tracking performance when the machine background will increase, as expected with increased luminosity.

5. Summary

The Silicon Vertex Detector is reliably providing high quality data since the start of the Belle II data taking in March 2019. With spatial resolution of 20μm, time resolution of 3ns, SNR within 13 to 33 and efficiency above 99%, years of development came to rewarding success.

6. Declaration of competing interest

The authors declare that they have no known competing financial interests or personal relationships that could have appeared to influence the work reported in this paper.

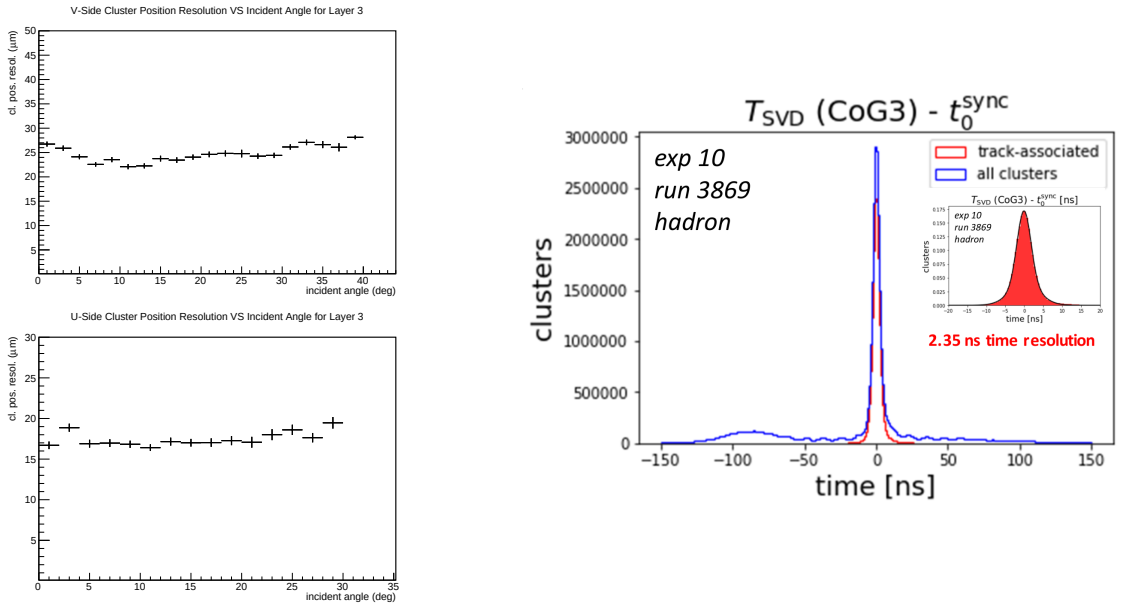

Figure 7: (Left) Spatial resolution of the layer 3 sensors as a function of the track incident angle for both sides. (Right) Hit time distribution and the resolution referenced to the event time. The bump below -60 ns is generated by off-time hits.

7. Acknowledgment

This project has received funding from the European Union's Horizon 2020 research and innovation programme under the Marie Skłodowska-Curie grant agreements No 644294 and 822070. This work is supported by MEXT, Japan, WPI, Japan, and JSPS (Japan); ARC (Australia); BMWFW (Austria); MSMT (Czechia); CNRS/IN2P3 (France); AIDA-2020 (Germany); DAE and DST (India); INFN (Italy); NRF, Republic of Korea-2016K1A3A7A09005605 and RSRI (Korea); and MNiSW (Poland).

References

[1] T. Abe, et al., Belle II technical design report, 2010, arXiv:1011.0352

[2] Y. Ohnishi, et al., Accelerator design at SuperKEKB, Prog. Theor. Exp. Phys. 2013 (3) (2013) 03A011, DOI:/10.1093/ptep/pts083

[3] M.J. French, et al., Design and results from the APV25, a deep sub-micron CMOS front-end chip for the CMS tracker, Nucl. Instrum. Methods Phys. Res. A 466 (2) (2001) 359–365, DOI:10.1016/S0168-9002(01)00589-7

[4] M. Friedl, et al., The origami chip-on-sensor concept for low-mass readout of double-sided silicon detectors, 2008, DOI:10.5170/CERN-2008-008.277

[5] L. Vitale, et al., The monitoring system of the belle II vertex detector, PoS Vertex2016 (2017) 051, DOI:10.22323/1.287.0051